Inclusions Chemistry for Mn/Si Deoxidized Steels: Thermodynamic Predictions and Experimental…

Article *in* ISIJ International · January 2004

DOI: 10.2355/isijinternational.44.1006

2 authors:

Youn-Bae Kang
Pohang University of Science and Technology
123 PUBLICATIONS **2,019** CITATIONS
SEE PROFILE

Hae-Geon Lee
Pohang University of Science and Technology
421 PUBLICATIONS **4,010** CITATIONS
SEE PROFILE

ISIJ International, Vol. 44 (2004), No. 6, pp. 1006–1015

Inclusions Chemistry for Mn/Si Deoxidized Steels: Thermodynamic Predictions and Experimental Confirmations

Youn-Bae KANG and Hae-Geon LEE

Dept. of Materials Science and Engineering

Pohang University of Science and Technology (POSTECH)

San-31, Hyoja-Dong, Nam-Ku, Pohang, 790-784, Korea

hglee@postech.ac.kr

ISIJ International, Vol. 44 (2004), No. 6, pp. 1006–1015

Abstract

Inclusions chemistry of Mn/Si deoxidized steel was studied through both thermodynamic computation and experimental method. The computational thermodynamics has proved to provide a powerful tool for controlling inclusions and precipitates in steel. For Mn/Si deoxidized steels, important factors in determining the liquidus temperature and primary phase of the inclusions are MnO/SiO_2 ratio and Al_2O_3 content in inclusions. Provided that no further interaction with steel matrix during cooling, inclusions having MnO/SiO_2 mass% ratio near unity and Al_2O_3 content in the range of 10 – 20 mass% give low liquidus temperatures (1150 – 1200°C) and primary phases of $MnSiO_3$ and $Mn_3Al_2Si_3O_{12}$ both which are soft. For the case of Mn + Si = 1.0 in mass%, the Mn/Si ratio of 2 – 5 meets the above conditions. Effect of the top slag on the inclusions chemistry can be predicted with accuracy, and hence it is possible to control the inclusions chemistry through proper design of the top slag composition so that the inclusions show a low liquidus temperature and soft primary phase. As the inclusions composition gradually changes with time toward the top slag composition, the length of refining time which determines the extent of reaction with the top slag is an important factor in determining the inclusions chemistry.

Keywords: inclusion; Mn/Si deoxidation; metal-inclusion reaction; the CaO-MnO-SiO_2-Al_2O_3 system; computational thermodynamics

1. Introduction

Complete removal of harmful inclusions from molten steel during the refining process is difficult to achieve. An alternative approach is to nullify or at least minimize the harmful effects of residual inclusions or to beneficially utilize these inclusions through proper control and modification. This alternative approach requires accurate knowledge in phase change and compositional relation of inclusions in steel under various chemical and thermal conditions during processing.

In Mn/Si deoxidation, the main constituents of inclusions are MnO and SiO_2. A small amount of Al_2O_3 may exist together. CaO may also come from interaction of the molten steel reacts with CaO-based top slag in a ladle or tundish. Many experimental studies[1-8] have been performed on MnO-Al_2O_3-SiO_2 inclusion systems. In addition, several thermodynamic calculations,[9-17] simply based on the activity of slag and interaction parameters of alloying elements (such as Mn, Si, Al and O) in steel, have been conducted in order to help control MnO-Al_2O_3-SiO_2 type of inclusions. However, the work reported so far has limited itself in its practical application to steel production: (1) the work has been done for limited compositional and thermal conditions which are not enough to cover conditions prevailing in actual steel production, and (2) more importantly the accuracy of the work is not high enough in many compositional and thermal conditions of the system so that a precise prediction and control of this type of inclusions are difficult to achieve.

Recently, thermodynamic modeling and database development for complex phase equilibria have been actively pursued by a number of researchers[18] which can also be applied to steelmaking processes to greatly assist in prediction and control with accuracy of

complex processes such as steel-slag-refractory reactions, changes in inclusion compositions, *etc*. As for Mn/Si deoxidized steels, thermodynamic approach will be of use to control and modify inclusions chemistry and phases, provided that thermodynamic databases for the system on hand be available and also reliable. Most previous researches focused mainly on activity-composition relations of liquid slag/inclusion and liquid steel.[9-17] Without simultaneous consideration of phase equilibria of an inclusion system on hand, however, thermodynamic approach will suffer its limitation for a practical application to steel production which experiences various thermal treatments such as solidification, cooling, reheating, etc.

The present work aims at investigation of phase and compositional relationships among liquid steel, slag and inclusions by employing both computational thermodynamics and experimental verification. Mn/Si deoxidized steel is chosen as the target steel, since it usually contains both liquid and solid inclusions during processing. For thermodynamic computations, a thermodynamic database for slag and inclusion, which was optimized by the present authors,[19-21] was used, and all calculations were performed using the FactSage® thermochemical software. [22]

2. Thermodynamic Basis – Models and Database

2.1. Liquid Steel

Most investigators have used interaction parameter formalism developed by Wagner[23] and extended by Sigworth and Elliot.[24] This formalism has been widely used in metallurgy to calculate activity/activity coefficients of solutes in liquid steel. Many experiments have

been conducted to evaluate interaction parameters among metallic elements, O, C, S, N *etc*. in molten iron and are well documented in the literature.[24,25] However, it fails sometimes to reproduce experimental data, particularly for those cases of 1) a highly concentrated region or 2) containing strong deoxidizer such as Al, Ca and Mg. In order to solve these problems in a thermodynamically sound way, Pelton and Bale[26-28] developed Unified Interaction Parameter Formalism (UIPM) which modifies Wagner formalism[23,24] and Darken formalism.[29] Moreover, in order to reproduce the deoxidation phenomena when strong deoxidizing elements exist, Jung *et al*.[30] proposed the use of associates such as Al*O, Ca*O, Si*O etc. in molten iron with UIPM. This UIPM with associates shows excellent agreement between calculation and experiments for deoxidation phenomena in liquid steel with a few model parameters.[30] Therefore, UIPM with associates was used to describe thermodynamic properties for liquid steel. All interaction parameters required for deoxidation of Mn, Si, Al and Ca were already evaluated by Jung *et al*.[30] and are used in this work.

2.2. Liquid Slag/Inclusion

Several thermodynamic models for liquid slag systems have been developed over several decades by many researchers and some of these have shown good reproducibility to experimental data and are convenient to use with a computer. In this work, the Modified Quasichemical Model[31,32] was used. This model takes into account short-range-ordering by considering second-nearest-neighbor pair exchange reactions. The details of this model are described in detail elsewhere.[31,32] All model parameters for CaO-MnO-SiO_2-Al_2O_3 systems

were already optimized by the present authors[21] and the details of thermodynamic optimization of this system and model parameters are described elsewhere.[21]

2.3. Solid Steel

Thermodynamic properties for solid steel such as FCC and BCC phases were calculated using the SGTE database.[33]

3. Experimental

The experimental apparatus employed in the present work is schematically shown in **Fig. 1**. A $MoSi_2$ electric resistance furnace connected to a proportional-integral-differential (PID) controller with a Pt/6%Rh-Pt/30%Rh thermocouple was used for all experiments in the present work.

Phase and chemistry of inclusions in equilibrium with a liquid steel were investigated in two different methods; namely, (1) direct formation of inclusions in the liquid steel and (2) equilibration of slag phase with the liquid steel. For the case of the former method, a master alloy with desired compositions (0.3kg) was prepared by melting predetermined amounts of high-purity electrolytic iron, Mn (99.99 mass%), Si (99.999 mass%) and Fe-1 mass% Al in a MgO crucible (40×10^{-3}m OD, 35×10^{-3}m ID, 130×10^{-3}m L) under a deoxidized argon atmosphere. After homogenization, this master alloy was quenched and then cut into pieces. Portion of the master alloy (0.04kg) is then placed in a small MgO crucible (25×10^{-3}m OD, 19×10^{-3}m ID, 50×10^{-3}m L) and an appropriate amount of Fe_2O_3 powder (99.9 mass%) was added as an oxygen source. The charged crucible was then positioned in the furnace and

held at 1550°C under an argon atmosphere. The argon was purified by passing it through an $Mg(ClO_4)_2$ column and a tube filled with Mg chips at 450°C. After holding for 30 minutes, the crucible was taken out of the furnace and quenched rapidly in a helium gas stream, followed by quenching in an iced-water. The top side of the quenched sample was sectioned, mounted, polished and finally subjected to observation of inclusions and measurement of their compositions. An electron probe micro analyzer (EPMA) with wave-length-dispersive (WDS) detectors (JEOL JXA-8100®) was used to measure inclusion compositions. An accelerating voltage of 15kV and a probe current 40nA were applied. Pure MnO, SiO_2 and Al_2O_3 supplied by JEOL Ltd. were used as standards for EPMA measurements.

For the latter method, master slags saturated by Al_2O_3 were prepared by melting the mixture of MnO, SiO_2 and Al_2O_3 in a Pt crucible. Then high-purity electrolytic iron (0.04kg) and appropriate amounts of Mn (99.99 mass%), Si (99.999 mass%), Fe-1mass% Al, Fe_2O_3 (99.9 mass%) were placed in an Al_2O_3 crucible (32×10^{-3}m OD, 28×10^{-3}m ID, 60×10^{-3}m L) together with the master slag (0.008kg). The crucible was then placed in the hot zone of the resistance furnace and equilibrated at 1600°C under a purified Ar atmosphere. Preliminary experiments showed that duration of 2 hours was enough to ensure the equilibrium of both liquid metal and liquid slag phases. In the case of high SiO_2 containing slags, the system was held for 4 hours to give an extra equilibration time. After quenching the whole crucible, metal and slag samples were subjected to chemical analysis. Si in metal and SiO_2 in slag were analyzed by the gravimetric method. Mn, Al in metal and MnO, Al_2O_3 in slag were analyzed by ICP emission spectrometry. Fe_tO in slag was analyzed by the titration method and the total oxygen in metal phase was analyzed using an

infrared absorption analyzer.

4. Results and Discussion

4.1. Characteristics of Inclusions in Mn/Si deoxidized Steel

It is desired to keep inclusions in a liquid state during the steel refining stage and to have any remaining inclusions soft enough during the rolling and plastic deformation stage. Liquid inclusions may form a glassy phase, depending on the cooling rate. Glassy inclusions are in general easily elongated during plastic deformation of the steel. For the case of Mn/Si deoxidation, therefore, the low liquidus region of the MnO-SiO_2-Al_2O_3 ternary oxide system is a good target for the inclusions chemistry. **Figure 2** is a diagram of the liquidus surface of the MnO-SiO_2-Al_2O_3 system optimized by the present authors.[19] It is seen that the liquidus temperature of the spessartite ($Mn_3Al_2Si_3O_{12}$) primary phase region and its close vicinity in the range of 1100°C~1200°C as indicated by thick line. It is known that the hardness of spessartite is low enough so that it can be easily deformed after crystallization from the liquid oxide.[34] Crystals containing low or no Al_2O_3 such as rhodonite ($MnSiO_3$) and tephroite (Mn_2SiO_4) also exhibit low hardness.[34,35] If one is satisfied with inclusions which lie in the 50 mass% liquid + 50 mass% solid two-phase region at 1200°C, the window for the target inclusion chemistry becomes much wider as shown in **Fig. 3**.

It is seen in Fig. 2 that the low liquidus temperature region lies in the MnO/SiO_2 ratio of 0.5 to 2 (in mass % basis). **Figure 4** shows the change of liquidus temperature as a function of Al_2O_3 content for fixed MnO/SiO_2 ratios (= 0.5, 1.0 and 2.0). Primary solid phases which appear first on cooling are also shown on the liquidus lines. Al_2O_3 content higher than 20

mass% in inclusions results in crystallization of alumina, mullite or galaxite ($MnAl_2O_4$). For the case of MnO/SiO_2 = 0.5 in mass % basis, the low liquidus region is narrow and the liquidus temperature is around 1,250ºC only in the vicinity of Al_2O_3 content of 20 mass%. The system of MnO/SiO_2 = 1, on the other hand, exhibits a wide low liquidus region, ranging from 5 to 25 mass% of Al_2O_3. In addition, the primary phase which precipitates out of the liquid in the region is either rhodonite or spessartite, both of which are soft.

4.2. Inclusions Generated by Deoxidation (MnO-SiO_2-Al_2O_3 type inclusion)

Formation of inclusions is governed by both steel chemistry and prevailing temperature. Mn/Si deoxidized liquid steel with a small amount of Al and O may produce inclusions of MnO-SiO_2-Al_2O_3 type. Reactions which prevail in the system will be,

$$\underline{Si} + 2\underline{O} = (SiO_2) \quad \text{……(1)}$$

$$\underline{Mn} + \underline{O} = (MnO) \quad \text{……(2)}$$

$$2\underline{Al} + 3\underline{O} = (Al_2O_3) \quad \text{……(3)}$$

When the system is in equilibrium,

$$K_{Si} = \frac{a_{SiO_2}}{a_{Si}a_O^2} \quad \text{……(4)}$$

$$K_{Mn} = \frac{a_{MnO}}{a_{Mn}a_O} \quad \text{……(5)}$$

$$K_{Al} = \frac{a_{Al_2O_3}}{a_{Al}^2 a_O^3} \quad \text{……(6)}$$

where K_i's are equilibrium constants of corresponding reactions and a_i is activity of component i. Eliminating the oxygen activity from the above equations, one can obtain,

$$a_{SiO_2} = K_{Si}\left(\frac{a_{Si}}{a_{Al}^{4/3}}\right)\left(\frac{a_{Al_2O_3}}{K_{Al}}\right)^{2/3} \quad \text{.....(7)}$$

$$a_{MnO} = K_{Mn}\left(\frac{a_{Mn}}{a_{Al}^{2/3}}\right)\left(\frac{a_{Al_2O_3}}{K_{Al}}\right)^{1/3} \quad \text{.....(8)}$$

Now, knowing the metal compositions (Si, Mn and Al) and temperature, one can solve the above equations of Eqs.(7) and (8) for oxides compositions with help of the following Gibbs-Duhem equation:

$$x_{SiO_2} d\ln a_{SiO_2} + x_{MnO} d\ln a_{MnO} + x_{Al_2O_3} d\ln a_{Al_2O_3} = 0 \text{ ....(9)}$$

Alternatively, the equilibrium conditions may be found by the so-called free energy minimization method, namely,

$$\frac{\partial G}{\partial n_{i,p}} = 0 \text{ .....(10)}$$

where G is the Gibbs free energy of the entire system, $n_{i,p}$ is the number of moles of the i-th component in the phase p, with mass balance equations in the system.

Figure 5 shows compositional relationship between the metal phase and oxide inclusions to be formed with constraints of Si + Mn = 1.0 mass% and T = 1550°C. In the figure the metal composition is given as the ratio of Mn/Si in mass% basis, Al (ppm) and O (ppm). It can be read from the figure that for a given Mn/Si ratio the composition of oxide inclusions should lie on the corresponding iso-Mn/Si ratio line. For example, in steel with Mn/Si = 1.0 the inclusions composition should lie on the line for Mn/Si = 1.0. The exact position on the line, in other words, the exact equilibrium composition of inclusions will be determined by additional information of Al or O content in the steel. One can also easily identify the range of metal compositions which can produce low liquidus inclusions by referring to Figs.2 and

5. Ideal metal composition for low liquidus inclusions is found to be in the range of Mn/Si = 2 – 5 for the constraint of Si + Mn = 1 mass% at 1550°C.

In order to verify the validity of the above results predicted through thermodynamic computations, experimental work was carried out for three different metal compositions, namely, Mn/Si = 0.1, 1.0 and 9, and results are given in **Fig. 6**. All data points in the figure are also listed in Table 1. Although data points show some scatter, most points tend to lie on corresponding iso-Mn/Si lines. Dispersion of the data points on an iso-Mn/Si line is attributed to local fluctuation of Al content which leads to variation of oxygen content. Referring to Fig. 5, a small variation of Al content may result in a large change of oxide compositions. Ogawa *et al.*[5] reported the composition of inclusions found in Mn/Si deoxidized tire-cord steel chemistry. **Figure 7** shows their results superimposed on the diagram predicted by thermodynamic computation with their steel chemistry and prevailing temperature (1580°C). Their data are in excellent agreement with the prediction.

4.3. Metal-Slag Equilibration

From thermo-chemical point of view there is no difference between slag and inclusions when equilibrated with steel. When the composition of inclusions in equilibrium with a steel is to be determined by equilibrating oxide slag with steel in a crucible, the slag is inevitably saturated with the crucible material. This method therefore imposes restriction to the variation of oxide composition. Nevertheless, this method enables to acquire oxide compositions saturated with the solid crucible material (for instance Al_2O_3, MgO or CaO) and in equilibrium with the steel.

In the present study, steel and oxide slag of a number of different compositions were equilibrated in an alumina crucible at 1600°C, and results are given in **Table 2**. In **Fig. 8** experimental slag compositions in equilibrium with steels are compared with thermodynamic predictions under the same conditions. The experimental results are seen to be in good agreement with the thermodynamic predictions. **Figure 9** shows slag compositions reported by Ohta *et al*.[4] and obtained by the present study where the total of mass% Si and mass% Mn is around 1. Numbers adjacent to the symbols indicate the Mn/Si ratio. It is clearly seen that the experimental results are represented with accuracy by the thermodynamic predictions given in the same figure.

Metal compositions in equilibrium with slag (inclusions) determined in the present study given in **Table 2** are graphically given in **Fig. 10**. Data reported by Ohta *et al*.[4] and Fujisawa *et al*.[3] are also included in the figure. Lines in the figure represent equilibrium relationship between the Mn/Si ratio and dissolved oxygen for given total concentrations of Si and Mn. The thermodynamic prediction reasonably well represents the experimental results except the case of low Si content, namely, Mn + Si = 0.5 and Mn/Si > 10. This disagreement is not immediately explainable, but tentatively attributed to uncertainty of chemical analysis of low concentration of Si. It should be noted that the thermodynamic database used in the present computations was optimized by separate studies by the present authors[21] and Jung *et al*.[30] Therefore, the calculation results presented in this paper are not a fitting, but solely prediction. Taking into account genetic uncertainties which are difficult to avoid in this type of experimental work, some data scatter shown in Fig. 10 may be considered acceptable.

Equilibrium phases of inclusions were thermodynamically determined at different compositions of Fe-Si-Mn-Al-O steel phase at 1550°C, and results are given as a kind of stability diagram in **Fig. 11**. It is seen that Mn exerts a large influence on stable phase. Increase in Mn content in steel greatly enlarges the liquid oxide area.

4.4. Effect of Top Slag

The composition of inclusions formed in Mn/Si deoxidized steel may be represented by the CaO-MnO-SiO_2-Al_2O_3 quaternary system. Al_2O_3 may come from ferroalloys which usually contain Al as an impurity, and CaO from the top slag. Once inclusions have been generated by deoxidation practice, their composition may gradually change through interaction, directly or indirectly, with the top slag. Change of inclusions composition along with elapse of refining time after deoxidation are plotted in a quasi-ternary phase diagram of CaO-MnO-SiO_2-Al_2O_3 quaternary system (5mass% and 15mass% Al_2O_3 sections) in **Figures 12(a)** and **12(b)**. The data in the figure are from actual plant operation.[36,37] It is seen that the initial composition of inclusions is gradually moving toward the top slag composition for both cases. This change may be simulated by thermodynamic considerations. First the initial inclusions are equilibrated with the steel, and then a small amount of the top slag is gradually added to the steel. In each addition thermodynamic equilibrium is computed to find a new composition of inclusions. Repeating this procedure enables to trace the compositional path which inclusions follow. The inclusions composition will eventually come close to that of the top slag. Lines in Fig. 12(a) and 12(b) are results of thermodynamic calculations. It can be seen that thermodynamic prediction

reasonably well reproduces the results of the plant data.

4.5. Phase Transformation of Inclusions During Cooling

Inclusions, liquid ones in particular, will experience phase transformation during casting and subsequent cooling of steel. The extent of phase transformation of inclusions will depend largely on the cooling rate. Thermochemical relationship between the steel and inclusions will be kept near equilibrium only if cooling proceeds at a sufficiently slow rate. Nevertheless, computation of equilibrium phases of inclusions at different temperatures will provide a useful tool to predict possible phases which inclusions may exhibit. **Figure 13** is the polythermal projection of the CaO-SiO_2-MnO quasi-ternary diagram sectioned at 15 mass% Al_2O_3 of the CaO-SiO_2-MnO-Al_2O_3 quaternary phase diagram. The shaded area has the same significance as that in Fig. 12(b). This phase diagram provides a clue as to what kind of crystal phase will first appear when a liquid oxide solution is cooled. Liquid inclusions whose composition lies in the hatched area in Fig. 13 will first crystallize into tridymite (SiO_2), anorthite ($CaAl_2Si_2O_8$) and wollastonite ($CaSiO_3$-$MnSiO_3$). Maeda *et al*.[36] actually found that the composition of most inclusions observed in as-cast bloom lied between wollastonite and the anorthite phase boundary and SiO_2 primary phase region.

To be more precise and accurate, however, mass transfer between the metal and oxide phases which might occur during cooling should be taken into consideration. On cooling, since solubility of oxygen in steel decreases with decreasing temperature, oxygen dissolved in the steel will move into liquid inclusions and form additional oxides with Mn, Si and Al that exist near the inclusions. The composition of the liquid inclusions will then change

during cooling, and hence the inclusions compositions will leave the phase diagram of Fig. 13 which is the section with constant Al_2O_3 at 15 mass%. In order to accommodate this mass exchange, the equilibrium relationship was computed for the whole system including both steel (Fe-Si-Mn-Al-O) and inclusions (SiO_2-MnO-Al_2O_3-CaO) phases at a number of different temperatures. Results for the initial compositions of inclusions represented by the points A, B and C in Fig.13 are shown in **Figures 14(a)**, **(b)** and **(c)**, respectively. In the figures, the amount of each phase is given relative to the amount of liquid inclusions that exist at 1550^{o}C. It is seen in Fig.14 that the amount of inclusions increases with decreasing temperature. This is due to the fact that those metallic elements of Al, Si, and Mn dissolved in the liquid steel at high temperatures become to react with dissolved oxygen to form oxides as the temperature decreases. The extent of change of the amount of inclusions with temperature in particular depends largely on the availability of oxygen in the metal. If a large amount of oxygen is available, then the change of the amount of inclusions with temperature will also be large. It is seen that the solid SiO_2 phase precipitates out of the liquid inclusions at a temperature below the liquidus, but above solidus of the steel. This implies that precipitation of SiO_2 is highly likely to occur even during a continuous cooling. Other phases such as wollastonite and anorthite are not likely to actually appear, as their precipitation temperatures are too low. Appearance of SiO_2 as inclusion is not desirable in general, since it is hard.[34,35)] As for the point B (Fig.14(b)) no solid phase will precipitate from liquid inclusions until the steel has been completely solidified. The first solid phase which appears by further cooling will be wollastonite, followed by anorthite. These solid phases are highly likely to precipitate out on continuous cooling, and, in particular, during

reheating of cast steel for hot rolling which normally occurs at around 1200°C. These solids are known soft so that they are elongated with ease along with the matrix steel during plastic deformation. As for the point C (Fig.14(c)), gehlenite tends to precipitate at a relatively high temperature and this solid phase is known hard.[35)]

4.5. Some Considerations on a Practical Application

Tirecord steel requires a tight control of inclusions/precipitates in terms of their size, morphology and chemistry. It is desired to control inclusions and precipitates in such a way that their physical properties are suitable to deform along with the steel matrix so that they do not exert an excessive stress or breakage during rolling or drawing. Al_2O_3 inclusion is hard and non-deformable, and deformability of inclusions of MnO-SiO_2-CaO-Al_2O_3 type is known to be influenced on the Al_2O_3 content to a large extent. For the case of MnO-SiO_2-Al_2O_3 type inclusions, proper control of the MnO/SiO_2 ratio enables the inclusions to exhibit low liquidus temperature and also to precipitate soft primary phases (see Fig. 4). Control of the MnO/SiO_2 ratio is in turn possible by adjusting Mn and Si contents in the steel. Ekerot[38)] reported that the deformability index (defined as the ratio of the strain of an inclusion to that of the steel) of MnO-SiO_2-Al_2O_3 inclusion shows a maximum at around 15 mass% of Al_2O_3. When CaO is included, which usually comes from interaction with the slag phase, the compositional range of liquid CaO-MnO-SiO_2-Al_2O_3 inclusions is greatly dependent on the Al_2O_3 content, as can be seen in Fig. 12. Maeda *et al.*[36)] reported that "Index of Undeformable Inclusion" in tirecord steel decreases as Al_2O_3 concentration increases, and exhibits the minimum at around 20 mass% of Al_2O_3, which is in agreement

with the result reported by Ekerot.[38] Thermodynamic computation therefore provides a powerful tool for finding an optimum composition of inclusions and for subsequent determination of steel chemistry which results in the optimum inclusion composition.

Suppose that a steel having the chemistry of 0.7C – 0.3Si – 0.7Mn (in mass%) is to be produced, and it is desired to optimize the slag chemistry so that inclusions can have a low liquidus temperature and precipitate soft primary phase(s). **Figure 15** shows results of thermodynamic computation on the liquidus temperature, primary phase and equilibrium oxygen content as a function of Al content in the aimed steel. It shows that, provided that there be no interaction with slag, formation of low-liquidus and soft inclusions ($Mn_3Al_2Si_3O_{12}$) is possible only at a very narrow range of Al content (1 – 1.7ppm). This kind of condition is difficult to achieve in practice, and, even if possible, the content of dissolved oxygen is too high (60 – 70ppm). This difficulty may be overcome by proper design of the top slag chemistry. Suppose that we have on hand a liquid steel containing 4ppm of Al and proper amount of O (51ppm) in equilibrium with Al_2O_3(s) inclusions at 1,550°C. When this steel is allowed to interact with a top slag at 1550°C, the chemistry of both the steel (O in particular) and inclusions will experience change. Results of some sample thermodynamic computations of the change are presented in **Fig. 16**. For the case of a hypothetical top slag of 55mass%CaO-45mass%SiO_2 (see Fig.16-a), the initial solid Al_2O_3 inclusions will be changed to become complex Al_2O_3-CaO-SiO_2 oxides as a result of interaction with the slag. As the metal-slag interaction proceeds, the content of CaO (and also that of SiO_2) in the inclusions will increase. The initial solid inclusions will then become liquid. The content of CaO in the inclusions (the abscissa in Fig. 16) can thus be

considered as the extent of interaction with the top slag. Let us consider the point A in Fig. 16(a) which represents an inclusion containing 25mass%CaO at 1550°C. This inclusion is fully molten, and its liquidus is 1311°C with the primary phase of $CaAl_2Si_2O_8$(anorthite). The equilibrium dissolved oxygen in the steel is now reduced to 40ppm. This reduction of oxygen potential is partly due to decrease of the activity of Al_2O_3 in the inclusions.

For inclusion engineering in Si/Mn deoxidation steels, those inclusions which have low liquidus temperatures and low hardness may be desirable. Needless to say, low oxygen content in steel is also desired. For low oxygen content in steel, increasing CaO content in inclusions is desirable as can be seen in Fig. 16. However, too high CaO content in liquid inclusions at 1550°C may result in high liquidus temperatures and undesirable solid primary phases such as Ca_2SiO_4 or $Ca_2Al_2SiO_7$ (see Fig. 16-b).

In order to predict inclusion behaviors during steel refining processes such as in ladles, RH degassers and tundish, much knowledge is required of kinetics, fluid dynamics, diffusion, solidification, thermodynamics, *etc*. However, steelmaking processes involve very high temperatures (> ~1550°C) so that chemical reactions can easily reach a thermodynamic equilibrium state. It is also confirmed in the present work that thermodynamics can predict many parts of inclusion behavior in steelmaking processes. Therefore, the prediction of a thermodynamic equilibrium state is the most important factor overall although dynamic flow of molten steel should be considered from fluid dynamics. Since CALPHAD[18] type thermodynamic calculations use a small size of thermodynamic data files and little computer resources, thermodynamic prediction which was conducted in the present work can be performed easily and accurately within a short time. This means

that this type of thermodynamic prediction for inclusion engineering can be a powerful tool to steelmaking plants and operators under practical operations.

6. Conclusions

Inclusions chemistry of Mn/Si deoxidized steel was studied through both thermodynamic computation and experimental confirmation. It has proved that the computational thermodynamics provides a powerful tool for engineering inclusions and precipitates in steel. The following is the summary of important findings in the present study:

(1) For Mn/Si deoxidized steel, MnO/SiO_2 ratio and Al_2O_3 content in inclusions are important factors in determining the liquidus temperature and primary phase of the inclusions.

(2) Provided that no further interaction with steel matrix during cooling, inclusions having MnO/SiO_2 mass % ratio near unity and Al_2O_3 content in the range of 10 –20 mass% give low liquidus temperatures (1150-1200^oC) and primary phases of $MnSiO_3$ and $Mn_3Al_2Si_3O_{12}$ both which are soft.

(3) It is possible to predict the inclusions composition from steel chemistry. For instance, in the case of Mn + Si = 1.0 in mass%, the Mn/Si ratio of 2 – 5 meets the above conditions.

(4) Effect of the top slag on the inclusions chemistry can be predicted with accuracy, and hence it is possible to control the inclusions chemistry through proper design of the top slag composition so that the inclusions show a low liquidus temperature and soft primary phase.

(5) As the inclusions composition gradually changes with time toward the top slag composition, the length of refining time which determines the extent of reaction with the top slag is an important factor in determining the inclusions chemistry.

Acknowledgements

A financial support from POSCO (Pohang, Korea) is gratefully acknowledged. The authors also thank to Prof. A. D. Pelton and Dr. I.-H. Jung (Ecole Polytechnique, Canada) for supporting database development and valuable discussions and Prof. W.-G. Jung (Kookmin Univ., Korea) for providing plant data.

REFERECES

1) H. Sakao: *Tetsu-to-Hagané*, **56** (1970), S621.

2) T. Fujisawa and H. Sakao: *Tetsu-to-Hagané*, **63** (1977), 1494.

3) T. Fujisawa and H. Sakao: *Tetsu-to-Hagané*, **63** (1977), 1504.

4) H. Ohta and H. Suito: *Metall. and Mater. Trans. B*, **27B**, (1996), 263.

5) K. Ogawa, T. Onoe, H. Matsumoto, K. Narita: *Tetsu-to-Hagané*, **71**, (1985), A.29.

6) D.H. Woo, Y.B. Kang and H.G. Lee: *Metall. and Mater. Trans. B*, **33B**, (2002), 915.

7) R.A. Sharma and F.D. Richardson: *Trans. TMS-AIME*, **233** (1965), 1586.

8) K.P. Abraham, M.W. Davies, J.L. Barton, and F.D. Richardson: *Acta Metall.*, **8** (1960), 888.

9) D. A. R. Kay and J. Junpu: *Proc. 3rd Int. Conf. on Molten Slags and Fluxes*, H. B. Bell, The Institute of Metals, Glasgow, (1989), 263.

10) H. Suito and R. Inoue: *ISIJ Int*., **36** (1996), 528.

11) X. B. Zhang, G. C. Jiang and K. D. Xu: *Calphad*, **21** (1997), 311.

12) X. Zhang and S. V. Subramanian: *Wire J. Int*., **32** (1999), 102.

13) X. Zhang and M. Subramanian: *Steelmaking Conf. Proc*., **85** (2002), 102.

14) H. Gaye, P. Rocabois, J. Lehmann and M. Wintz: *Proc. of the Alex McLean Symposium*, The Iron & Steel Society, Toronto, (1998), 67.

15) S. Kobayashi: *ISIJ Int*., **39** (1999), 664.

16) L. C. Oertel and A. C. Silva: *Calphad*, **23** (1999), 379.

17) V. C. Galindo, R. D. Morales, J. A. Romero, J. F. Chaves, M. V. Toledd: *Steel Res*., **71** (2000), 107.

18) CALPHAD (CALculation of PHAse Diagrams): The International Research Journal for Calculation of Phase Diagrams.

19) I.H. Jung, Y.B. Kang S. A. Decterov and A. D. Pelton: *Metall. and Mater. Trans.*, (2002), accepted.

20) Y.B. Kang, I.H. Jung, S.A. Decterov, A.D. Pelton and H.G. Lee: submitted to ISIJ.

21) Y.B. Kang, I.H. Jung, S.A. Decterov, A.D. Pelton and H.G. Lee: accepted to ISIJ.

22) C.W. Bale, P. Chartrand, S.A. Degterov, G. Eriksson, K. Hack, R. Ben Mahfoud, J. Melançon, A.D. Pelton and S. Petersen: *Calphad*, 26 (2002), 189

23) C. Wagner: *Thermodynamics of Alloys*, Addison-Wesley, Reading, MA, (1962), 51.

24) G.. K. Sigworth and J. F. Elliott: *Met. Sci.*, **8** (1974), 298.

25) *Steelmaking Data Sourcebook*, Japan Society for the Promotion of Science, 19th Comm. on Steelmaking, Gordon & Breach Science, New York, NY, 1988.

26) A.D. Pelton and C.W. Bale: *Metall. Trans. A.* **17** (1986), 1211.

27) C.W. Bale and A.D. Pelton: *Metall. Trans. A.* **21** (1990), 1997.

28) A.D. Pelton: Metall. *Mater. Trans. B.* **28** (1997), 869.

29) L.S. Darken: *TMS-AIME*, **239** (1967), 90.

30) I.H. Jung, S.A. Decterov and A.D. Pelton: *Metall. and Mater. Trans*., (2002), accepted.

31) A.D. Pelton and M. Blander: *Metall. Trans. B*, **17** (1986), 805.

32) A.D. Pelton, S.A. Decterov, G. Eriksson, C. Robelin and Y. Dessureault: *Metall. Mater. Trans. B*, **31** (2000), 651.

33) SGTE (Scientific Group Thermodata Europe) solution database.

34) R. Kiessling: *Non-Metallic Inclusions in Steel*, The Iron and Steel Institute, (1968).

35) J.Kawahara, K.Watanabe, T.Banno and M.Yoshida: *Wire J. Internat.*, **11** (1992), 55.

36) S. Maeda, T. Soejima, T. Saito, H. Matsumoto, H. Fujimoto and T. Mimura: *Steelmaking Conf. Proc.*, **72** (1989), 379.

37) Plant Operation Data at #1 Steelmaking Plant, Pohang, Korea, private communication, 1997.

38) S. Ekerot: Scand. *J. Metall*. **3**, (1974), 21.

ISIJ International, Vol. 44 (2004), No. 6, pp. 1006–1015

Table 1. EPMA measurement results for inclusion composition from “direct formation of inclusions in the liquid steel”.

Mn/Si	SiO_2(wt%)	MnO(wt%)	Al_2O_3(wt%)	Mn/Si	SiO_2(wt%)	MnO(wt%)	Al_2O_3(wt%)
9	34.71	41.92	23.36	1	59.13	28.12	12.75
9	34.29	42.34	23.37	1	65.12	22.10	12.78
9	34.89	42.56	22.55	1	80.87	14.37	4.76
9	37.85	46.51	15.64	1	87.30	9.36	3.34
9	36.31	45.40	18.29	1	47.69	2.20	50.11
9	77.06	21.54	1.40	1	95.21	3.51	1.28
9	32.62	40.28	27.10	1	65.61	22.84	11.55
9	33.34	41.45	25.21	1	98.14	1.81	0.05
9	99.92	0.05	0.03	1	97.23	2.44	0.33
9	99.84	0.15	0.01	1	77.75	18.79	3.46
9	99.74	0.21	0.04	1	53.71	26.52	19.77
9	34.98	41.87	23.15	1	58.98	26.54	14.48
9	33.64	41.81	24.55	1	95.74	3.18	1.09
9	34.32	41.81	23.88	1	54.33	25.84	19.83
9	33.91	41.64	24.45	1	49.83	24.75	25.42
9	34.22	42.76	23.02	1	83.17	10.67	6.16
9	99.85	0.13	0.02	1	77.90	15.39	6.71
9	36.76	44.34	18.90	1	55.71	29.75	14.54
9	33.32	40.87	25.81	1	63.51	36.49	0.00
9	34.76	43.98	21.26	1	96.91	3.09	0.00
0.1	16.72	2.52	80.76	1	55.94	44.06	0.00
0.1	6.31	1.98	91.71	1	76.02	18.25	5.74
0.1	7.89	0.83	91.28	1	81.07	14.21	4.72
0.1	87.80	5.64	6.56	1	51.98	30.32	17.70
0.1	84.17	6.41	9.42	1	50.34	30.65	19.02
0.1	58.57	6.47	34.96	1	52.22	31.36	16.41
0.1	68.58	9.31	22.11	1	51.64	31.19	17.17
0.1	91.60	2.85	5.56	1	67.31	21.96	10.74
0.1	7.94	2.23	89.84	1	69.26	20.59	10.15
0.1	1.71	3.87	94.41	1	60.32	29.12	10.57
1	83.13	13.27	3.61	1	52.25	33.51	14.25
1	53.36	30.29	16.35	1	78.51	15.89	5.59
1	55.02	30.67	14.30	1	84.28	11.57	4.16

Table 2. Equilibrium compositions of metal and slag phase at 1600°C.

No.	Time in hour	Metal						Slag			
		[Mn]	[Si]	[Al]	[O] in ppm			(MnO)	(SiO_2)	(Al_2O_3)	(Fe_tO)
		Mass pct		ppm	Max.	Min.	Avg.	Mass pct			
1	2	0.643	0.019	5.0	72.9	71.1	72.1	31.2	23.9	41.1	3.9
2	2	0.686	0.028	6.4	64.0	62.7	63.3	30.6	24.3	41.4	3.6
3	2	0.399	0.045	9.6	61.2	59.5	60.5	25.5	31.1	39.4	4.1
4	4	0.280	0.377	10.2	56.8	53.5	55.5	22.1	37.0	36.7	4.2
5	4	0.290	0.433	7.2	52.5	51.1	51.8	21.9	37.8	36.8	3.5
6	2	0.911	0.082	11.8	52.8	51.1	51.9	36.0	22.0	39.3	2.6
7	2	0.991	0.100	19.7	44.1	43.2	43.8	33.8	24.2	39.7	2.6
8	2	0.664	0.598	24.7	46.5	38.7	44.0	26.8	32.4	40.8	-
9	4	0.357	0.662	10.3	36.3	34.9	35.7	23.1	38.1	36.4	2.5
10	4	0.376	0.775	6.9	36.2	35.2	35.6	21.8	38.6	36.6	3.0
11	2	1.389	0.118	11.6	38.2	36.7	37.2	35.1	22.4	40.3	2.2
12	2	1.565	0.540	13.1	33.3	29.2	31.0	34.3	24.4	39.7	1.6
13	2	1.008	0.964	18.5	32.2	28.4	30.3	29.2	31.2	38.1	1.4
14	4	0.577	1.368	21.3	30.4	29.7	30.1	23.5	37.7	37.1	1.8
15	4	0.571	1.480	15.2	28.5	28.0	28.2	21.9	39.6	36.6	1.9

List of Figures

Fig. 1. Schematic figure of the experimental apparatus

Fig. 2. Calculated liquidus surface of the MnO-SiO_2-Al_2O_3 system. (temperature in degrees Celsius)

Fig. 3. Calculated liquidus and two-phase regions with liquid mass proportion of 50% in a MnO-SiO_2-Al_2O_3 system at 1200°C.

Fig. 4. Calculated liquidus temperatures in the MnO-SiO_2-Al_2O_3 systems as a function of Al_2O_3 concentration. MnO/SiO_2 weight ratios are 0.5, 1.0 and 2.0, respectively.

Fig. 5. Compositional relationships between the metal and liquid oxide phases at 1550°C. Solid lines, dashed lines and dotted lines represent Mn/Si mass ratio, iso-oxygen and iso-aluminum in metal, respectively.

Fig. 6. Comparison between experiments and calculations of inclusion compositions in Mn/Si deoxidized steel at 1550°C. Mn + Si in steel is 1 mass %. All lines are calculated from the thermodynamic model.

Fig. 7. Comparison between experiments and calculations of inclusion compositions in high carbon Mn/Si deoxidized steel at 1580°C. Mn + Si in steel is 1 mass %. All lines are calculated from the thermodynamic model.

Fig. 8. Agreement between experimental and calculated compositions for the MnO-SiO_2-Al_2O_3 slag in equilibrium with metal. Sample No. in horizontal axis corresponds to those in **Table 2**.

Fig. 9. Comparison between experiments and calculation of inclusion compositions in Mn/Si deoxidized steel at 1600°C. All lines are calculated from the thermodynamic model. Numbers adjacent to experimental points means Mn/Si weight ratio in liquid steel.

Fig. 10. Compositional relationships between log(wt%Mn / wt%Si) and oxygen content in liquid steel with alumina (or mullite) saturation (a) at 1600°C and (b) at 1550°C.

Fig. 11. Calculated inclusion stability diagram in the Fe-Mn-Si-Al-O system at 1550°C for (a) mass% Mn = 0, (b) mass% Mn = 0.5, (c) mass% Mn = 1.0 and (d) mass% Mn = 1.5. Numbers adjacent to each line represent equilibrium oxygen content (in ppm) in liquid steel.

Fig. 12. Comparisons between reported data and thermodynamic calculation of the change of inclusion compositions during ladle arc refining process. Al_2O_3 concentration in inclusion is about (a) 5wt% and (b) 15wt%. All lines are calculated and thin lines represent liquidus lines in the CaO-MnO-SiO_2-Al_2O_3 system at 1550°C. Solid diamonds represent the composition of ladle slag.

Fig. 13. A calculated polythermal projection of the CaO-MnO-SiO_2-Al_2O_3 system sectioned at Al_2O_3 mass% of 15. The shaded area has the same meaning as that in Figure 12(b).

Fig. 14. Calculated phase transformation of steel and inclusion cooled from (a) point **A**, (b) point **B** and (c) point **C** in Figure 13. Amount of each phase is relative to the amount of liquid oxide at 1550°C (mass of each phase/mass of liquid oxide at 1550°C).

Fig. 15. Effect of Al concentration in liquid steel (0.7wt% C – 0.7wt% Mn – 0.3wt% Si) at 1550°C on the liquidus temperature/primary phase of inclusion, equilibrium oxygen content and Al_2O_3 concentration in liquid inclusion.

Fig. 16. Effect of top slag compositions on equilibrium oxygen content at 1550°C and liquidus temperature/primary phase of inclusion in equilibrium with the steel initially containing 4ppm Al (see Fig.15). Top slag compositions are (a) 55wt% CaO - 45wt% SiO_2, (b) 52.5wt% CaO - 40wt% SiO_2 - 7.5wt% Al_2O_3 and (c) 50wt% CaO - 35wt% SiO_2 - 15wt% Al_2O_3, respectively.

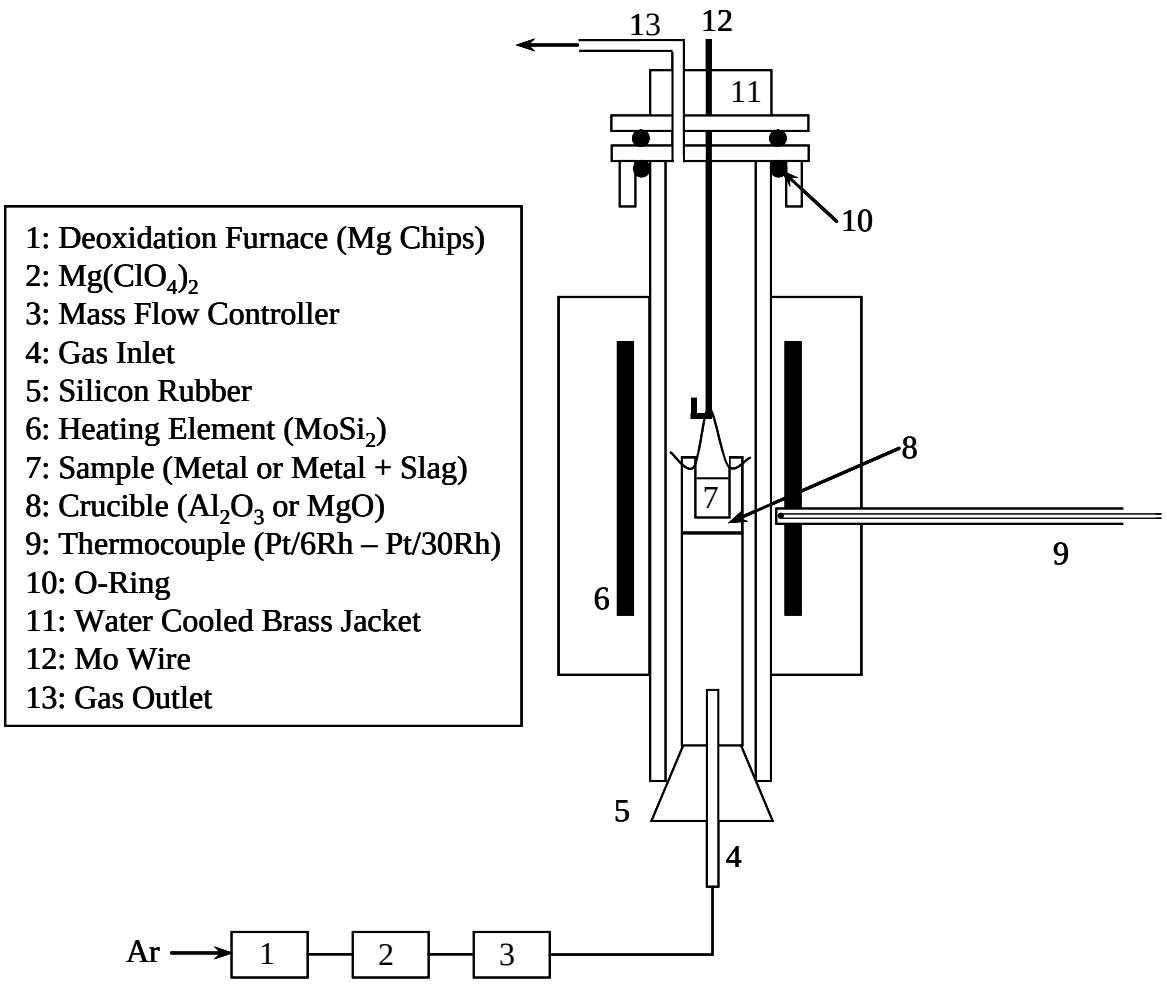

Fig. 1. Schematic figure of the experimental apparatus

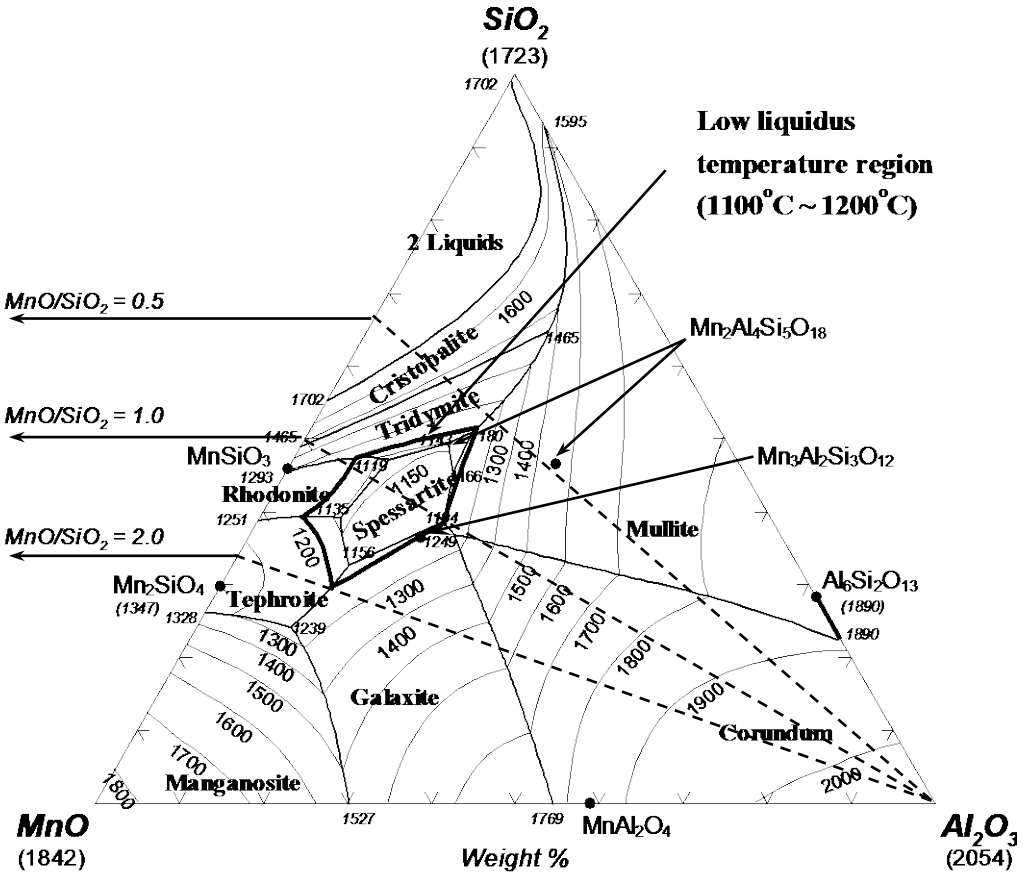

Fig. 2. Calculated liquidus surface of the MnO-SiO_2-Al_2O_3 system. (temperature in degrees Celsius)

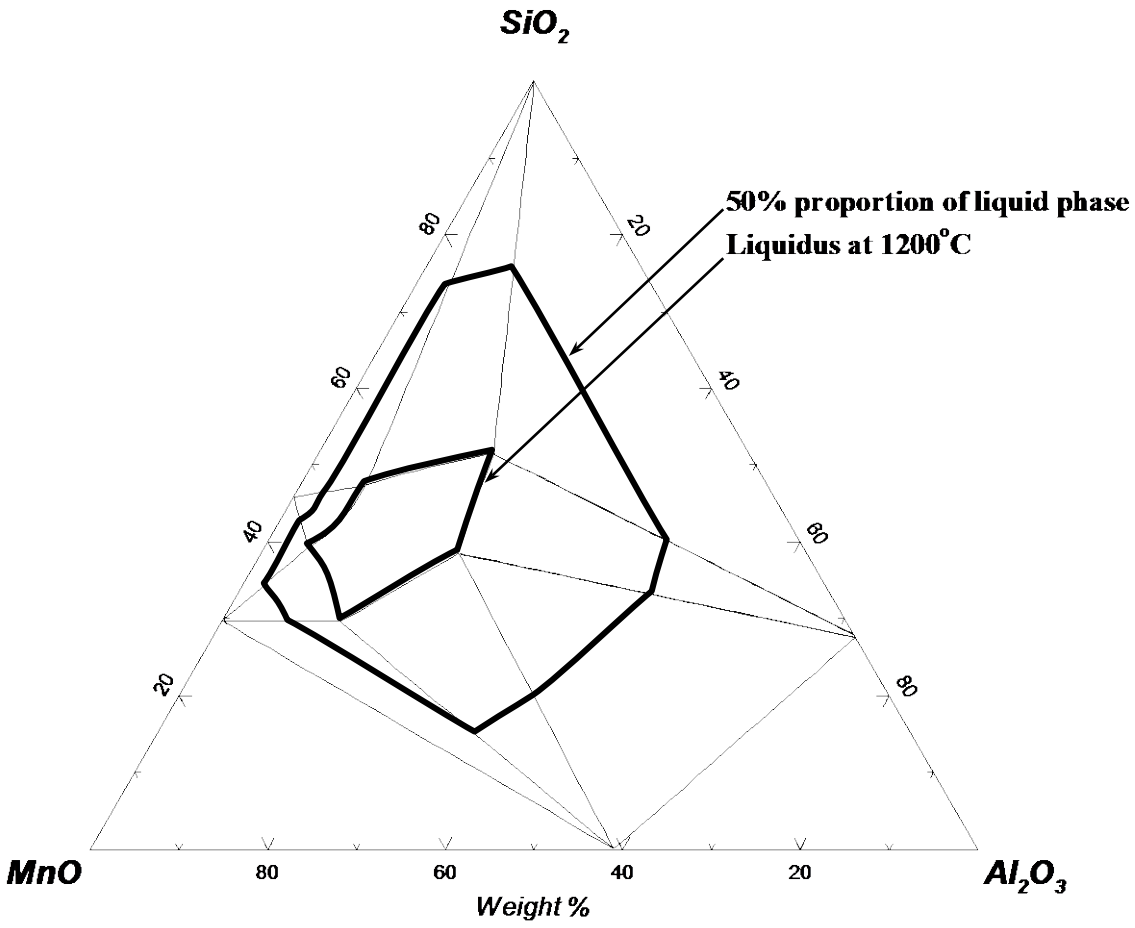

Fig. 3. Calculated liquidus and two-phase regions with liquid mass proportion of 50% in a MnO-SiO_2-Al_2O_3 system at 1200°C.

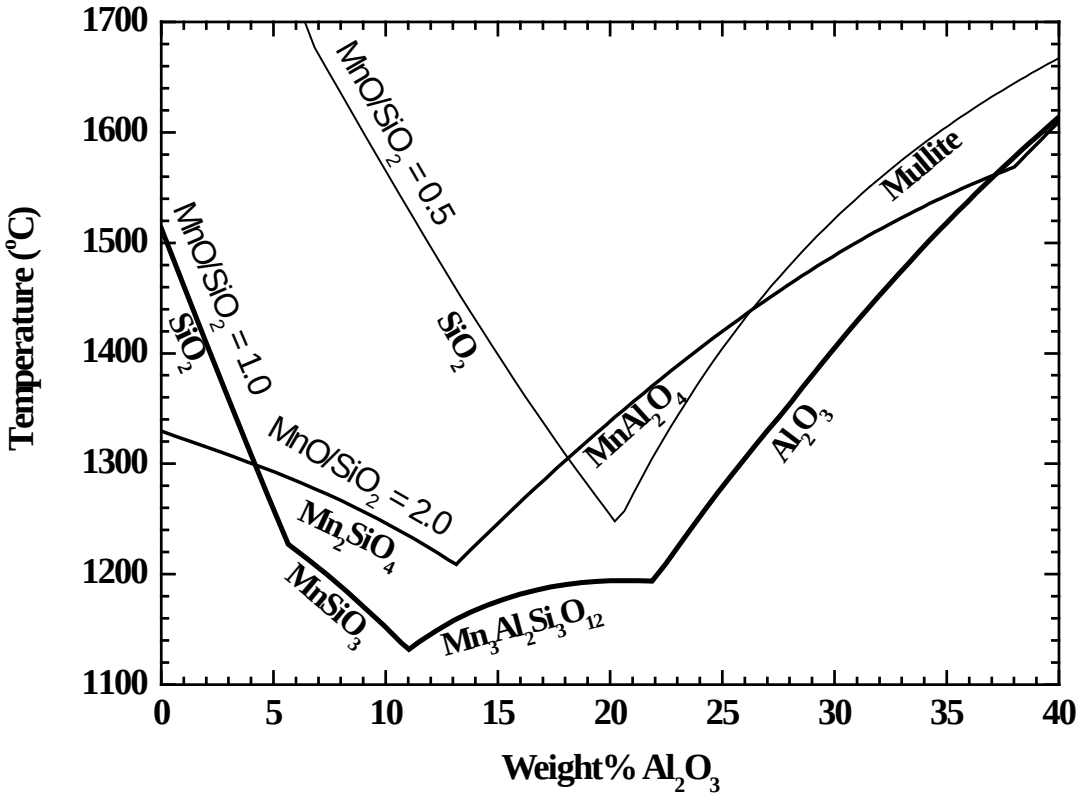

Fig. 4. Calculated liquidus temperatures in the MnO-SiO_2-Al_2O_3 systems as a function of Al_2O_3 concentration. MnO/SiO_2 weight ratios are 0.5, 1.0 and 2.0, respectively.

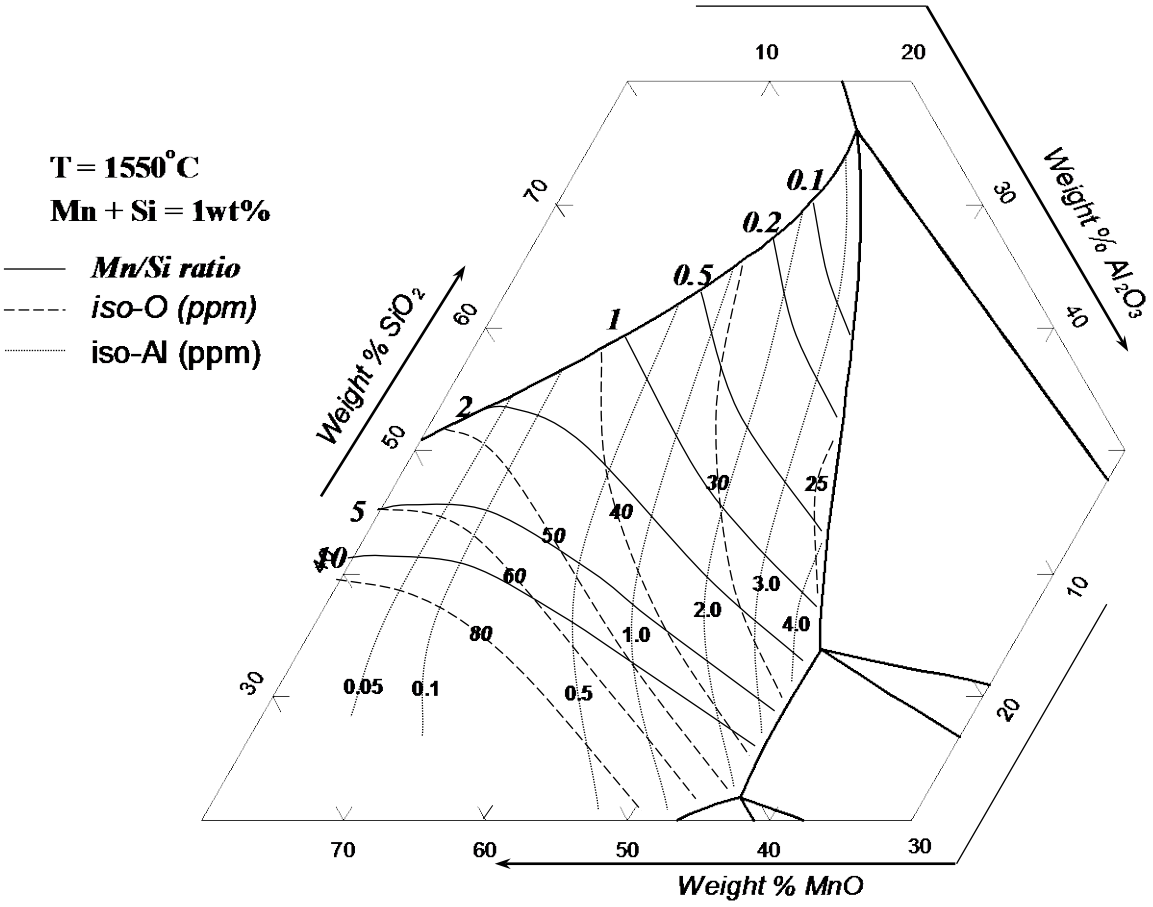

Fig. 5. Compositional relationships between the metal and liquid oxide phases at 1550°C. Solid lines, dashed lines and dotted lines represent Mn/Si mass ratio, iso-oxygen and iso-aluminum in metal, respectively.

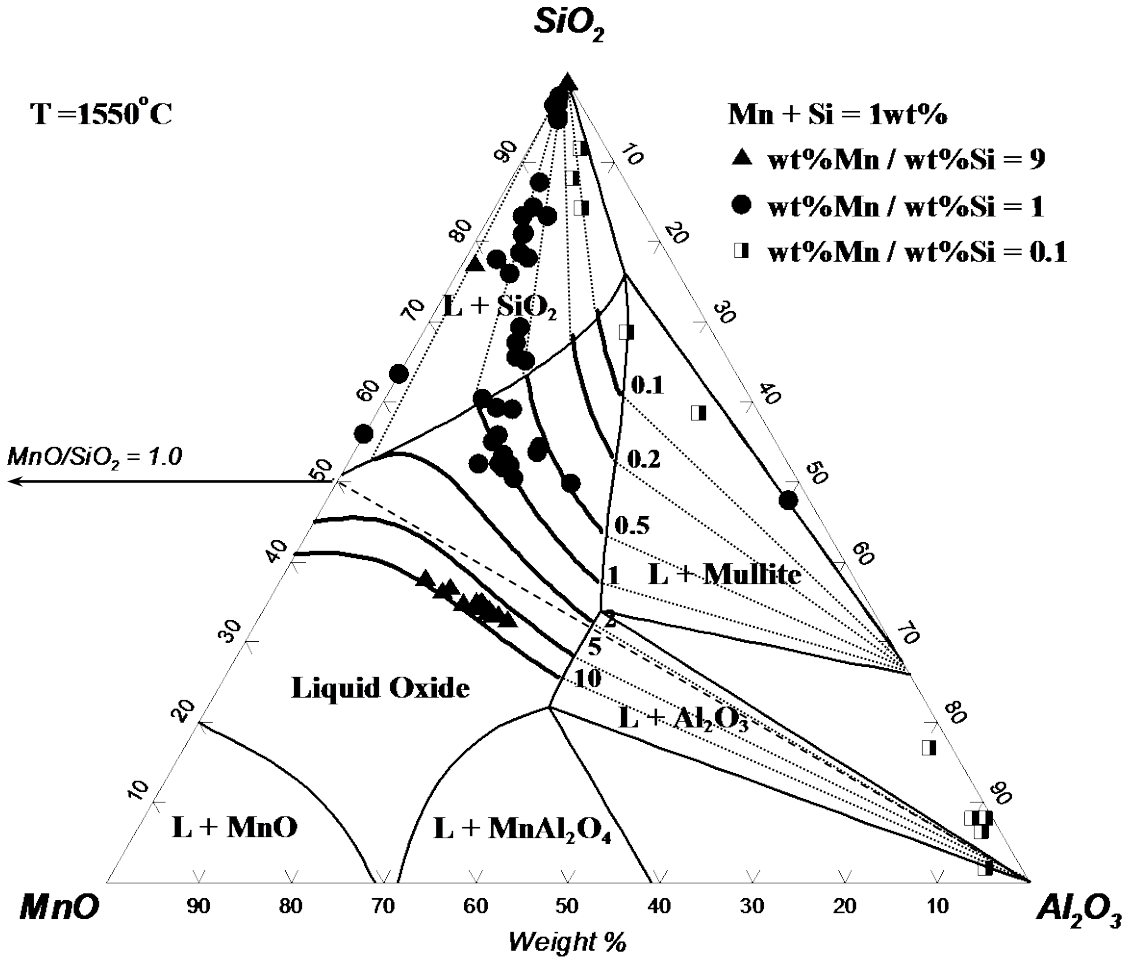

Fig. 6. Comparison between experiments and calculations of inclusion compositions in Mn/Si deoxidized steel at 1550°C. Mn + Si in steel is 1 mass %. All lines are calculated from the thermodynamic model.

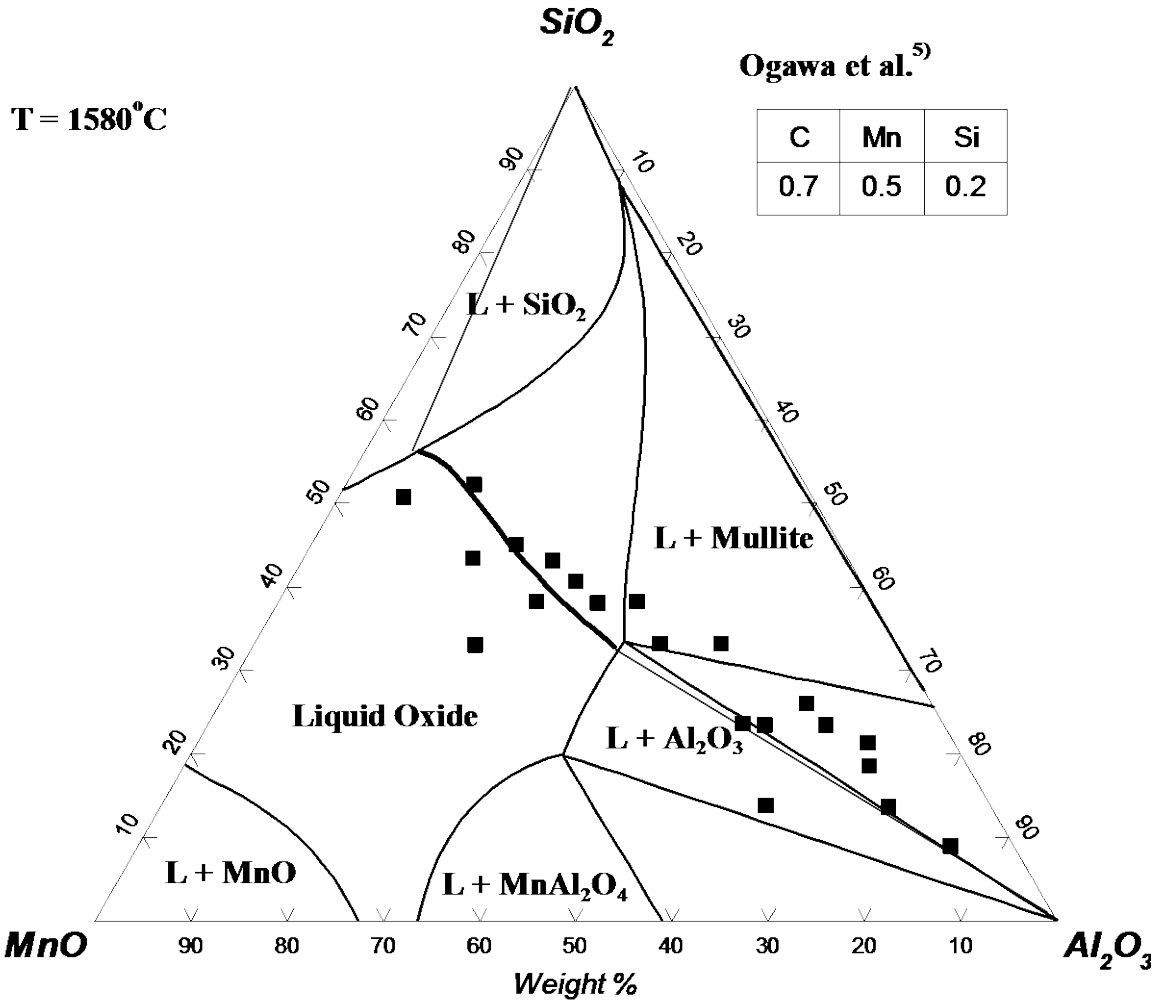

Fig. 7. Comparison between experiments and calculations of inclusion compositions in high carbon Mn/Si deoxidized steel at 1580°C. All lines are calculated from the thermodynamic model.

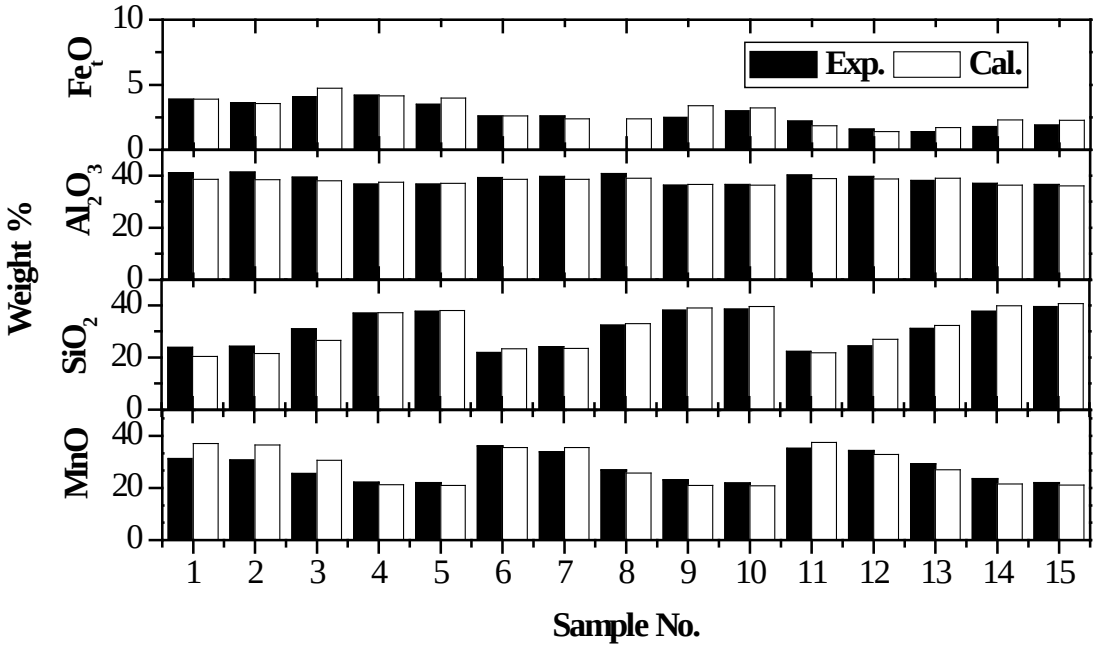

Fig. 8. Agreement between experimental and calculated compositions for the MnO-SiO_2-Al_2O_3 slag in equilibrium with metal. Sample No. in horizontal axis corresponds to those in **Table 2**.

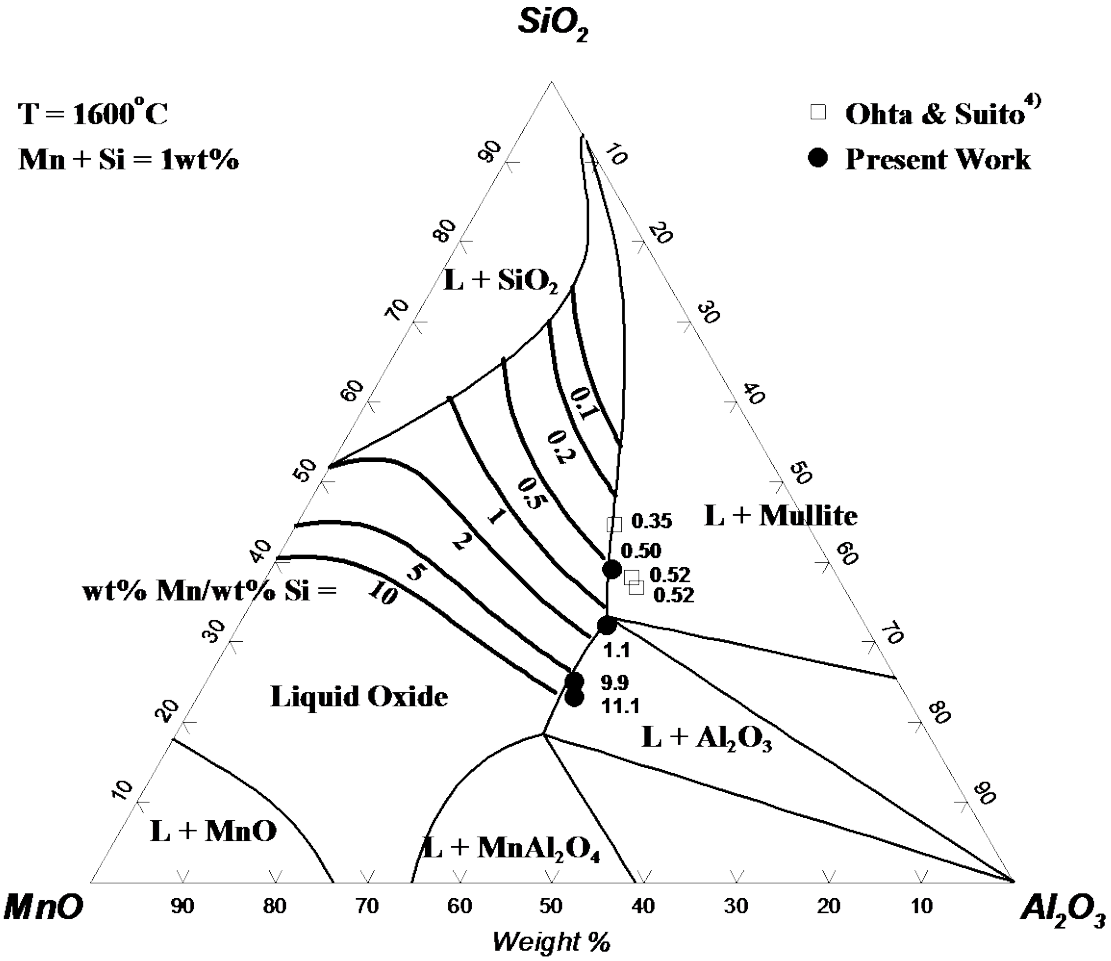

Fig. 9. Comparison between experiments and calculation of inclusion compositions in Mn/Si deoxidized steel at 1600°C. Mn + Si in steel is 1 mass %. All lines are calculated from the thermodynamic model. Numbers adjacent to experimental points means Mn/Si weight ratio in liquid steel.

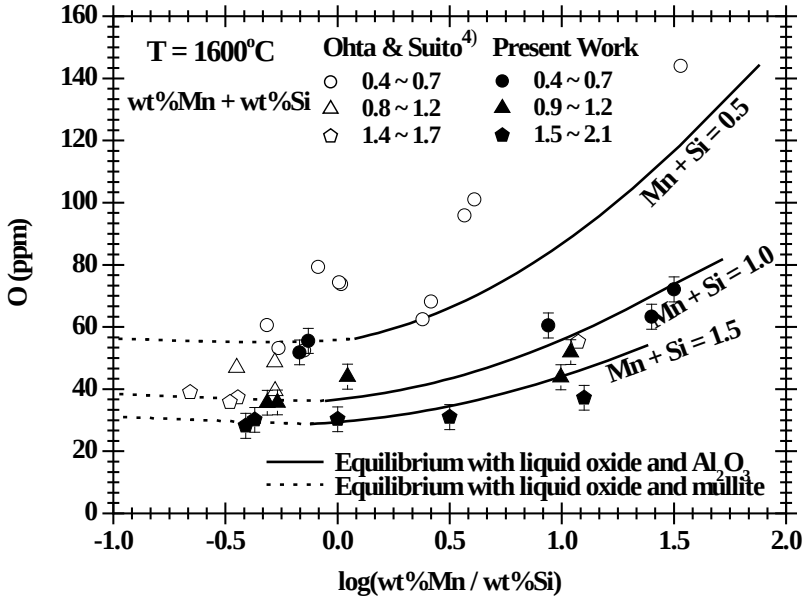

(a)

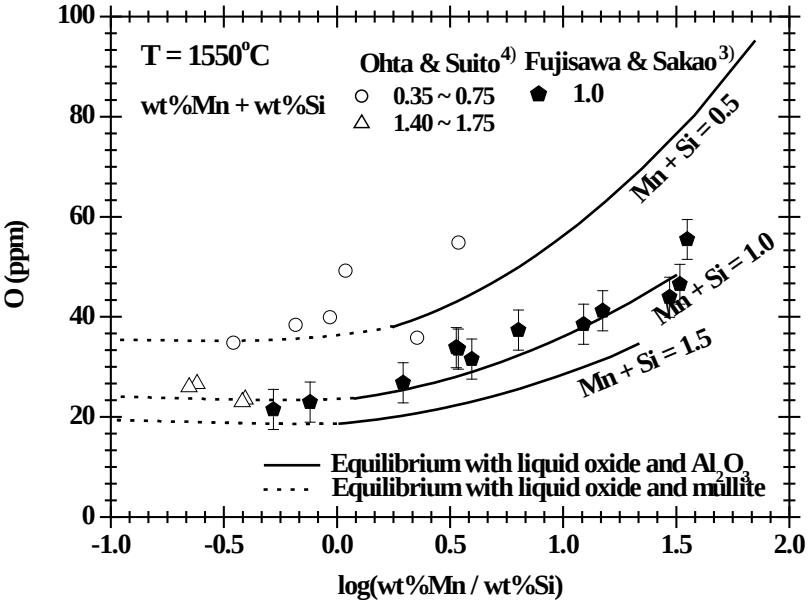

(b)

Fig. 10. Compositional relationships between log(wt%Mn / wt%Si) and oxygen content in liquid steel with alumina (or mullite) saturation (a) at 1600°C and (b) at 1550°C.

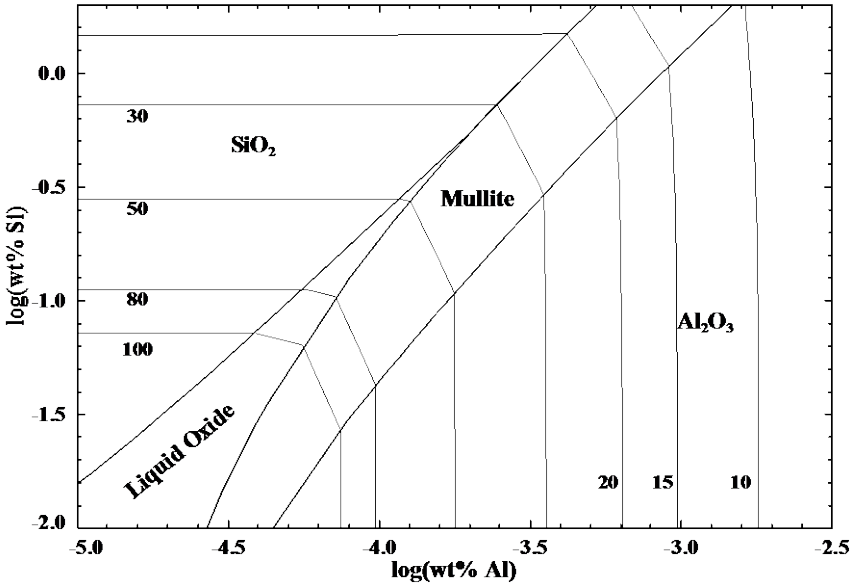
0.0
-0.5
-1.0
-1.5
-2.0
log(wt% Si)
-5.0
-4.5
-4.0
-3.5
-3.0
-2.5
log(wt% Al)
30
50
80
100
SiO2
Mullite
Al2O3
Liquid Oxide
20
15
10

(a)

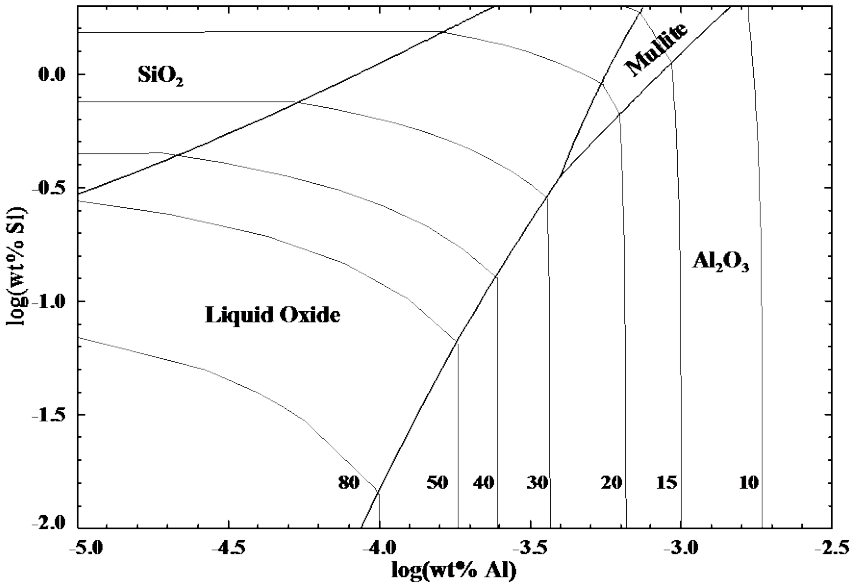
0.0
-0.5
-1.0
-1.5
-2.0
log(wt% Si)
-5.0
-4.5
-4.0
-3.5
-3.0
-2.5
log(wt% Al)
SiO2
Mullite
Al2O3
Liquid Oxide
80
50
40
30
20
15
10

(b)

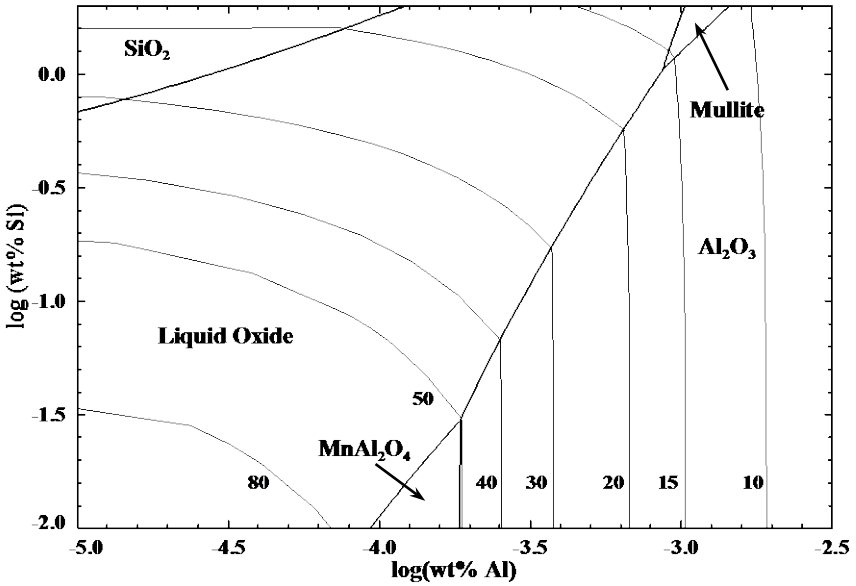

(c)

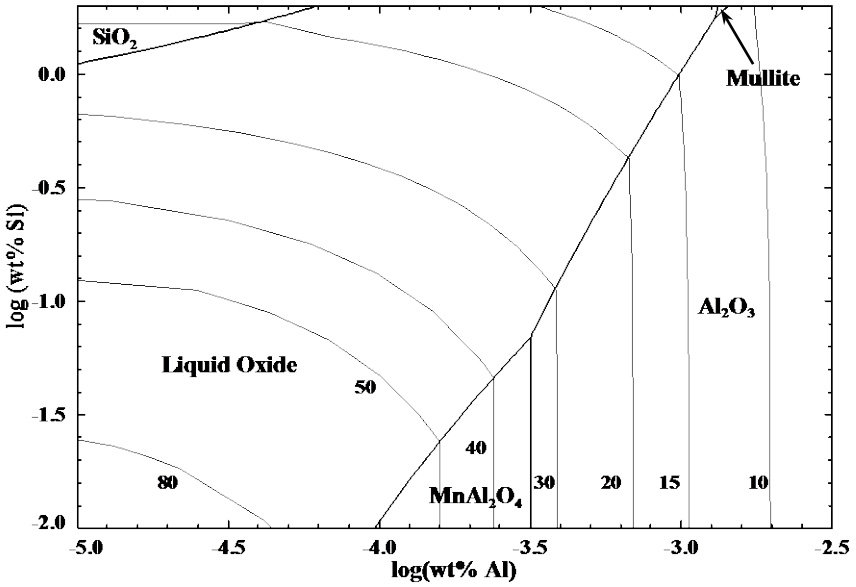

(d)

Fig. 11. Calculated inclusion stability diagram in the Fe-Mn-Si-Al-O system at 1550°C for (a) mass% Mn = 0, (b) mass% Mn = 0.5, (c) mass% Mn = 1.0 and (d) mass% Mn = 1.5. Numbers adjacent to each line represent equilibrium oxygen content (in ppm) in liquid steel.

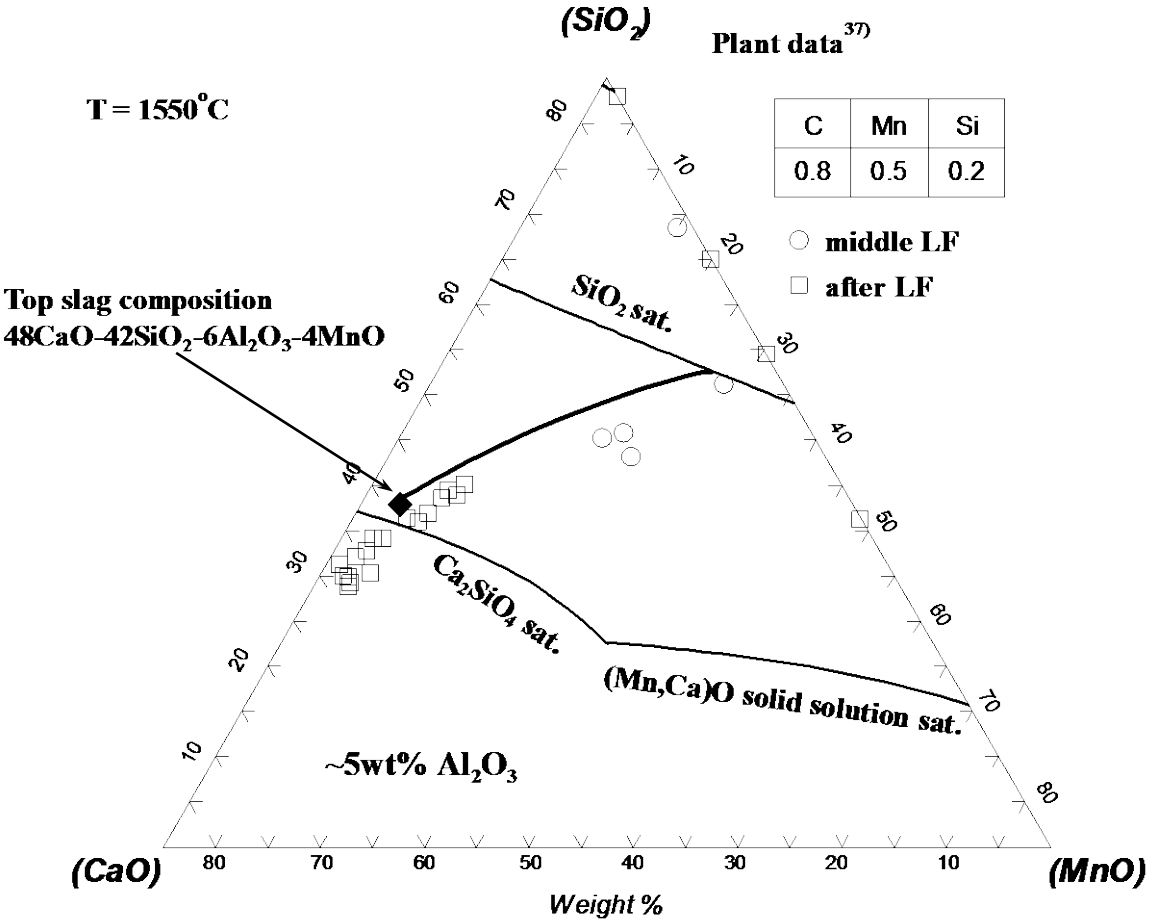
(SiO2)
Plant data37)
T = 1550°C
C Mn Si
0.8 0.5 0.2
middle LF
after LF
Top slag composition
48CaO-42SiO2-6Al2O3-4MnO
SiO2 sat.
Ca2SiO4 sat.
(Mn,Ca)O solid solution sat.
~5wt% Al2O3
(CaO)
(MnO)
Weight %

(a)

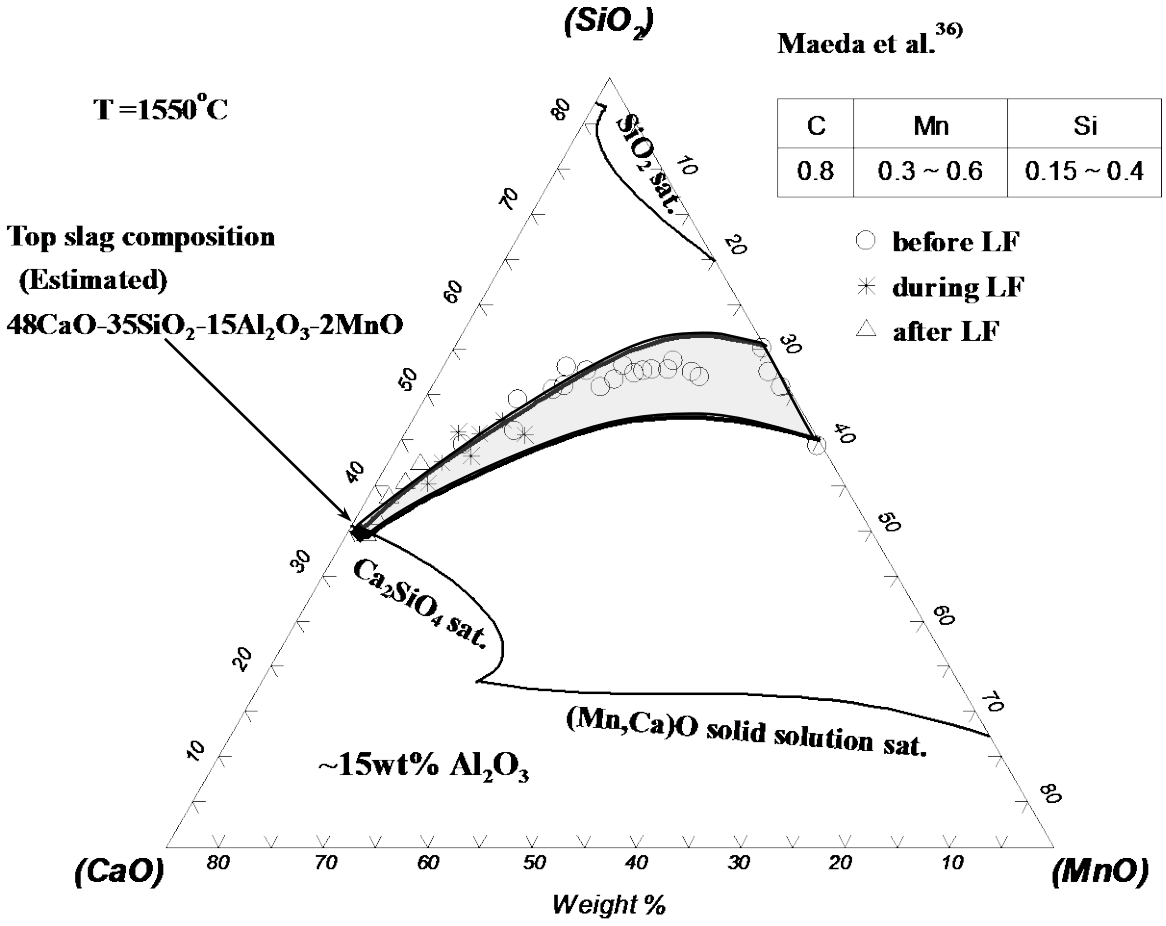

(b)

Fig. 12. Comparisons between reported data and thermodynamic calculation of the change of inclusion compositions during ladle arc refining process. Al_2O_3 concentration in inclusion is about (a) 5wt% and (b) 15wt%. All lines are calculated and thin lines represent liquidus lines in the CaO-MnO-SiO_2-Al_2O_3 system at 1550ºC. Solid diamonds represent the composition of ladle slag.

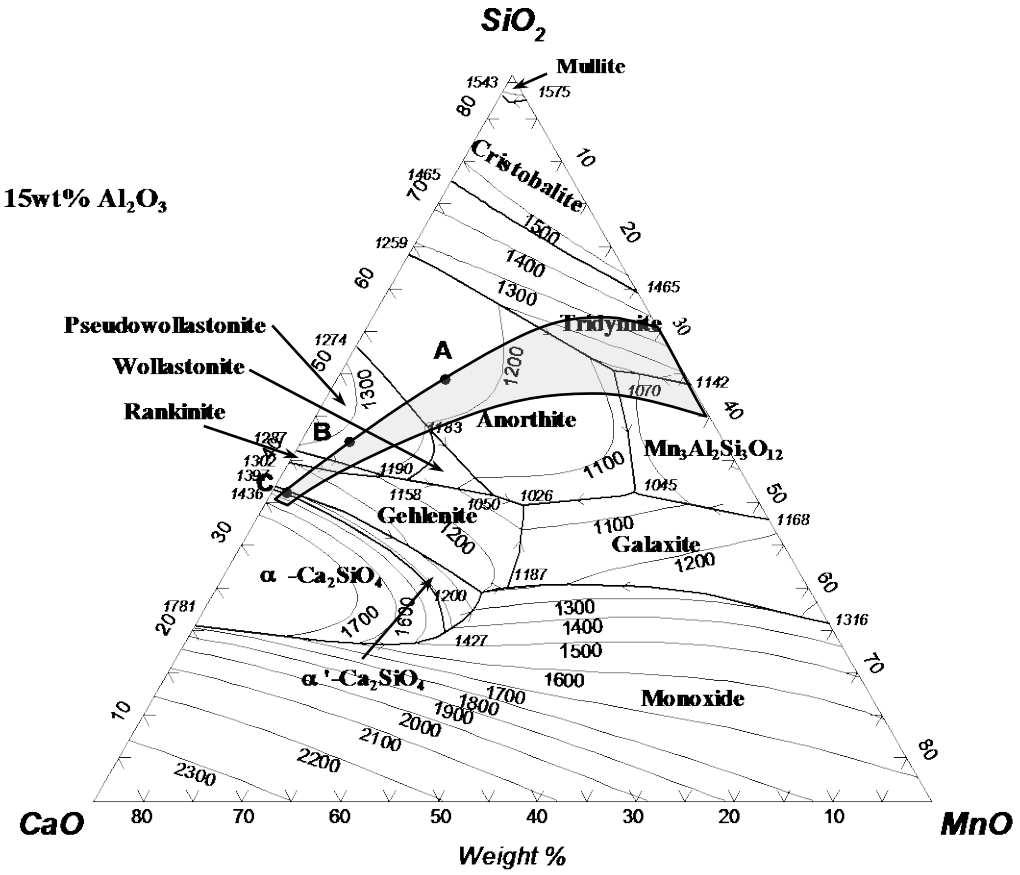

Fig. 13. A calculated polythermal projection of the CaO-MnO-SiO_2-Al_2O_3 system sectioned at Al_2O_3 mass% of 15. The shaded area has the same meaning as that in Figure 12(b).

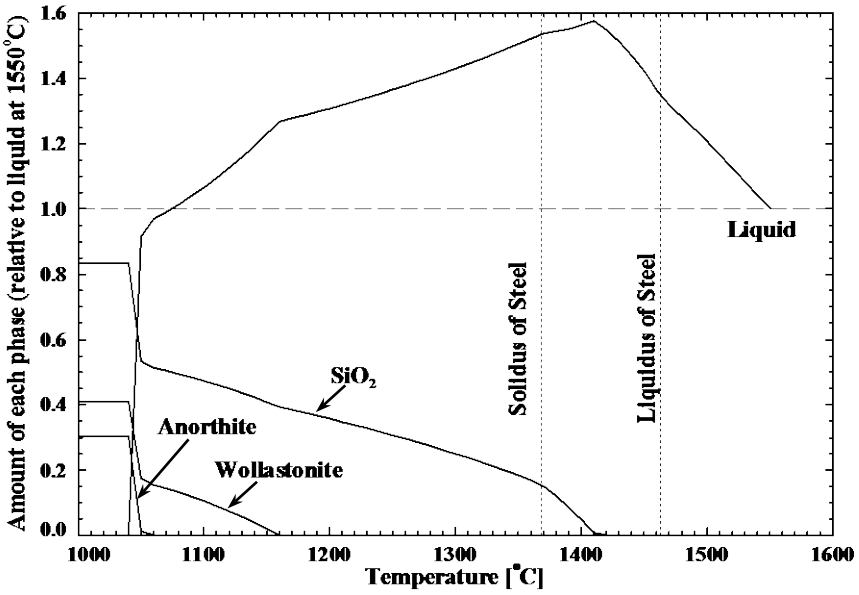
Amount of each phase (relative to llquld at 1550°C)
Temperature [°C]
Liquid
Solldus of Steel
Llquldus of Steel
SiO2
Anorthite
Wollastonite

(a)

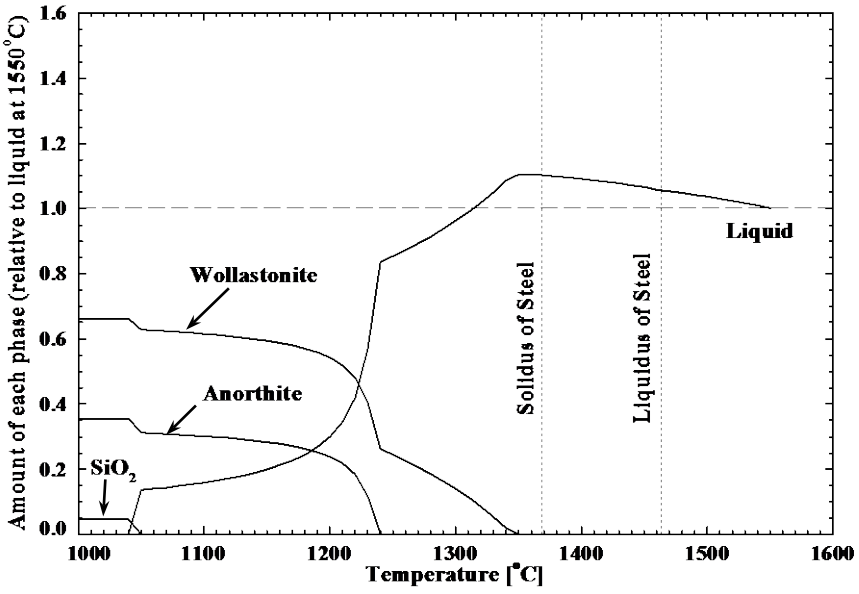
Amount of each phase (relative to llquld at 1550°C)
Temperature [°C]
Liquid
Wollastonite
Anorthite
SiO2
Solldus of Steel
Llquldus of Steel

(b)

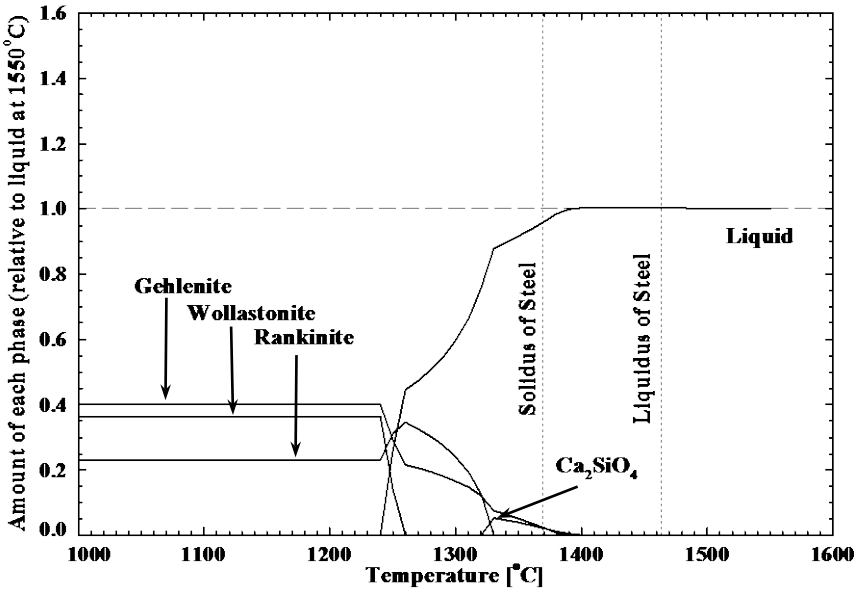

(c)

Fig. 14. Calculated phase transformation of steel and inclusion cooled from (a) point **A**, (b) point **B** and (c) point **C** in Figure 13. Amount of each phase is relative to the amount of liquid oxide at 1550°C (mass of each phase/mass of liquid oxide at 1550°C).

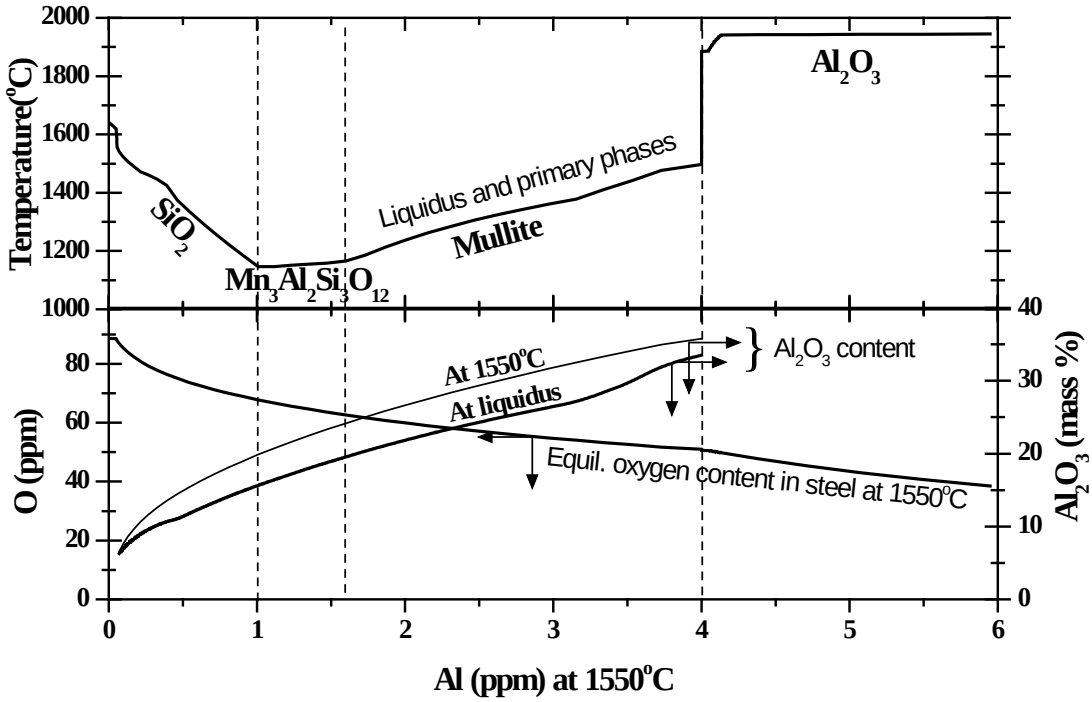

Fig. 15. Effect of Al concentration in liquid steel (0.7wt% C – 0.7wt% Mn – 0.3wt% Si) at 1550°C on the liquidus temperature/primary phase of inclusion, equilibrium oxygen content and Al_2O_3 concentration in liquid inclusion.

ISIJ International, Vol. 44 (2004), No. 6, pp. 1006–1015

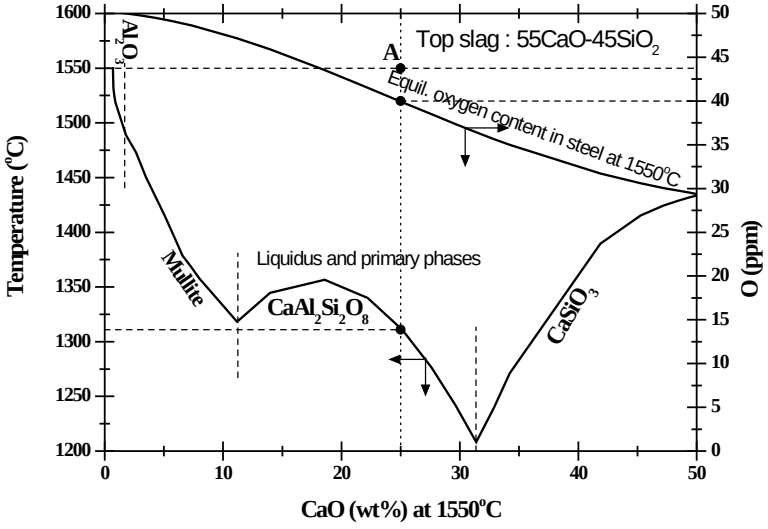

(a)

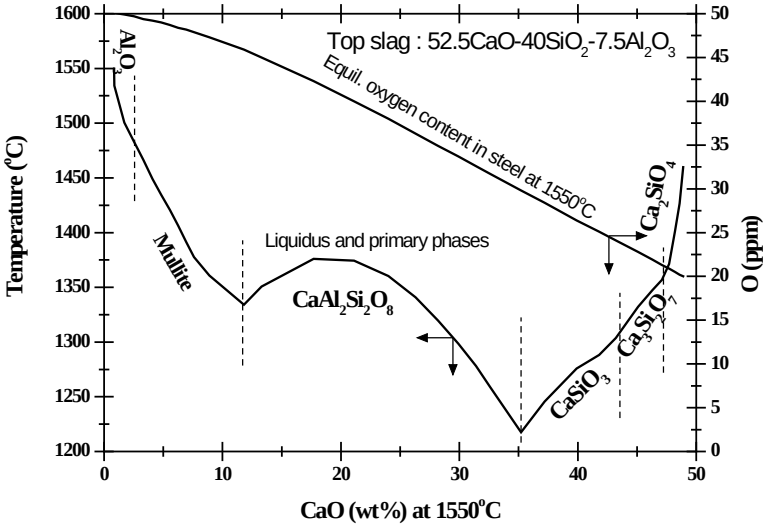

(b)

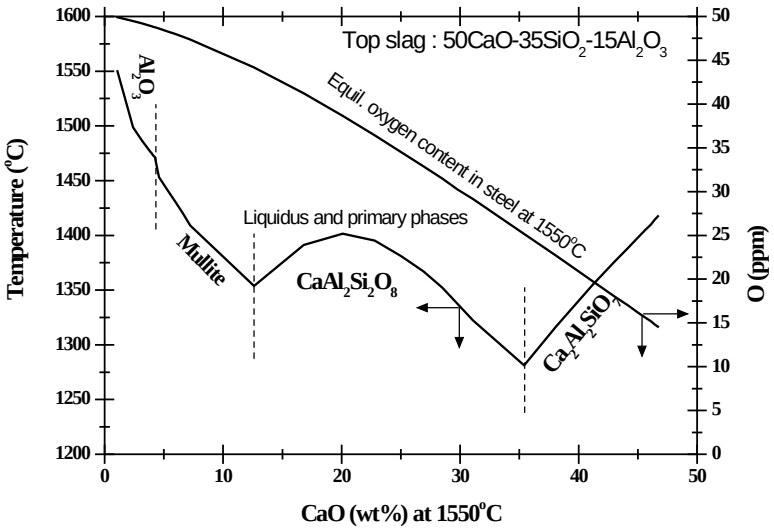

(c)

Fig. 16. Effect of top slag compositions on equilibrium oxygen content at 1550°C and liquidus temperature/primary phase of inclusion in equilibrium with the steel initially containing 4ppm Al (see Fig.15). Top slag compositions are (a) 55wt% CaO - 45wt% SiO_2, (b) 52.5wt% CaO - 40wt% SiO_2 - 7.5wt% Al_2O_3 and (c) 50wt% CaO - 35wt% SiO_2 - 15wt% Al_2O_3, respectively.